MODELING OF SOLAR CELLS

by

Balaji Padmanabhan

A Thesis Presented in Partial Fulfillment
of the Requirements for the Degree
Master of Science

ARIZONA STATE UNIVERSITY

November 2008

MODELING OF SOLAR CELLS

by

Balaji Padmanabhan

has been approved

November 2008

Graduate Supervisory Committee:

Dragica Vasileska, Chair
Dieter K. Schroder
Denis Mamaluy

ACCEPTED BY GRADUATE COLLEGE

ABSTRACT

Solar energy is becoming one of the primary sources of energy replacing fossil fuels due to its abundance. Its versatility, abundance and environmental friendly have made it one of the most promising renewable sources of energy. Solar cells convert this solar energy into Electrical Energy used to drive various appliances. The effort to improve the efficiency of these cells and the reduction of their costs has been a major concern for a long time. Modeling of various structures of solar cells provides an insight into the physics involved in its operation and better understanding of the ways to improve their efficiency.

In this work a three dimensional Drift Diffusion Model has been developed and has been used to simulate Silicon Solar cells. This model involves the self consistent solution of the Poisson and Continuity Equations. A pn silicon solar cell has been simulated to test the working of the code. Later a p+-p-n+ and n+-p-p+ structure of various lengths has been simulated to understand the physics behind the operation of a realistic silicon solar cell. Recombination mechanisms which play a crucial role in the determination of the cell efficiency such as Radiative Recombination, SHR recombination, Auger Recombination have been included in the code.

Light does not enter through all the regions of the device since the top metal contact has some reflectivity and thus prevents the light to enter the device called the Shadowing effect. Thus Shadowing effect tends to reduce the efficiency of the solar cell as the effective number of electron hole pairs generated within the device has been reduced and this is observed during simulation. The surface recombination effect has also

been included for the surface of the window through which light enters the device and this also tends to reduce the efficiency.

Finally the efficiency variation with the variation in the length of the device has been simulated. Theoretically the efficiency increases initially with the increase in the base length since the capture of higher wavelength photons or lower energy photons is possible thus increasing the efficiency but with increase after a certain length a decrease in the efficiency takes place due to the increase in the ratio of the length of the device to the diffusion length. In this work the increase in the efficiency with length has been simulated but the length could not be increased a lot to observe the decrease in efficiency due to limitation of simulation time.

Dedicated to my parents,

Mr. M. Padmanabhan and Ms. P. Rohini

And my elder sister,

P.Krishnaveni

.

ACKNOWLEDGMENTS

TABLE OF CONTENTS

LIST OF FIGURES

Chapter 1

INTRODUCTION

I.   ALTERNATIVE SOURCES OF ENERGY

Sun provides enormous amounts of energy powering oceans, atmospheric currents, and cycle of evaporation and drives river flow, hurricanes and tornadoes that destroy natural landscape. The San Francisco earthquake of 1906, with magnitude 7.8, released an estimated 10^{17} joules of energy which sun delivers in one second. Earth's resource of oil mounts up to 3 trillion barrels containing 1.7×10^{22} joules of energy that the sun supplies in 1.5 days. Humans annually use about 4.6×10^{20} joules annually which sun supplies in one hour. The sun continuously supplies about 1.2×10^{25} terawatts of energy which is very much greater than any other renewable or non renewable sources of energy can provide. This energy is much greater than the energy required by human beings which is about 13 terawatts. By covering 0.16% of Earth's land with 10% efficient solar cells would provide 20 Terawatts of energy about twice of fossil fuel consumption of the world including numerous nuclear fission reactors [1].

Solar energy is in abundance but only a little is used to directly power human activities. About 80%-85% of our total energy comes from fossil fuels. These resources are non renewable, fast depleting, produce greenhouse gases and other harmful environmental pollutants [2]. Threat to climate is one of the main concerns in adopting any resource as a primary source of energy. Fossil Fuels emit a large volume of green house gas like CO_2 into the atmosphere and disturb the ecological balance. These emissions have been increasing due to overutilization of fuels to meet the ever expanding

needs of human society. The solutions for this problem are to use fossil fuels in conjunction with carbon sequestration, nuclear power and solar power. Carbon sequestration is an extremely difficult method since a large volume of space is required to store the emitted green house gases and its maintenance is a very crucial issue. Nuclear power seems to be a good option but the feasibility of deploying several thousands of 1Gegawatt power plants all over the world to meet the 10Tera watt demand of the society is skeptical. The Uranium resource for these power plants on earth also gets exhausted in this process in about 10 years after which the processing of sea water has to be adopted which is also exhaustible and difficult. On the other hand shifting the focus on renewable sources of energy is the ideal choice and solar power is by far the most prominent energy source owing to its versatility, inexhaustible and environmental friendly features [1].
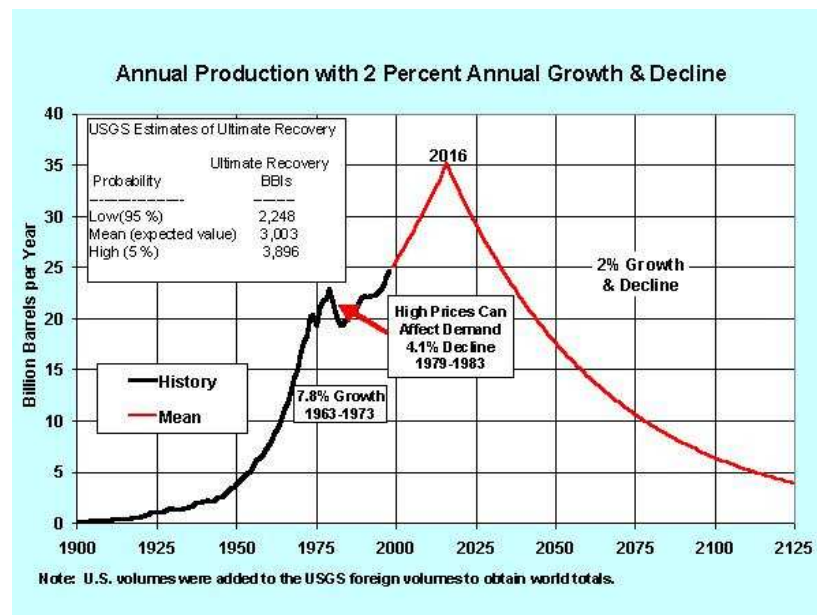
Figure 1.1 Annual Production of Oil [3]

The exhaustible nature of fossil fuels has also pushed us into the adoption of renewable sources of energy as the future. Fig1.1 shows the plot of the annual production of oil Vs year with a 2% annual growth and decline rate. We observe that these estimates show a very steep decline of this resource after the year 2016 thus demanding the need for an alternative source of energy [3]. The burgeoning solar cell market is maturing to become a very profitable investment to industries resulting in an annual growth of 41% in the last five years [4].
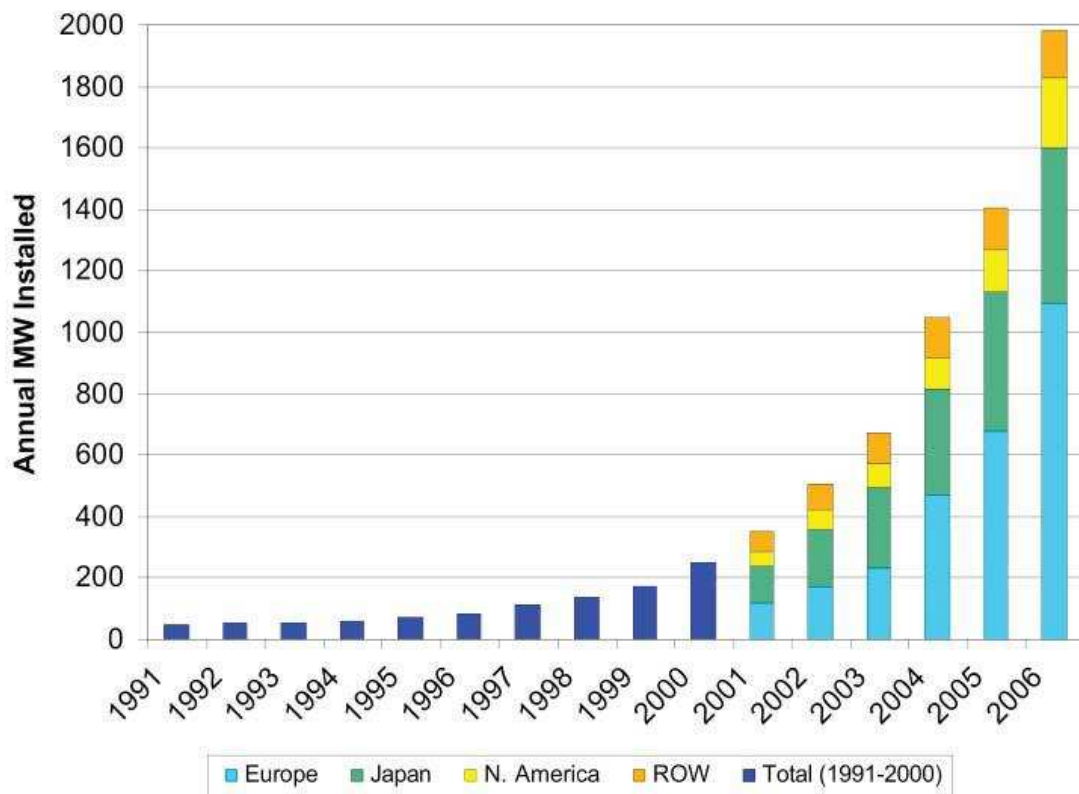
Figure 1.2 Global PV Installations by Year [4].

High costs and conversion efficiency have been the major bottlenecks in the potential of solar power becoming a primary source of energy. Nowadays major research done with the motive of improving the efficiency of these cells has brought this dream closer to reality. New methods of harnessing the full spectrum of the sun's wavelength, mutlijunction solar cells (homojunctions and heterojunctions), and new materials for making solar cells are paving way for solar power to be the emerging power resource for the world at large.
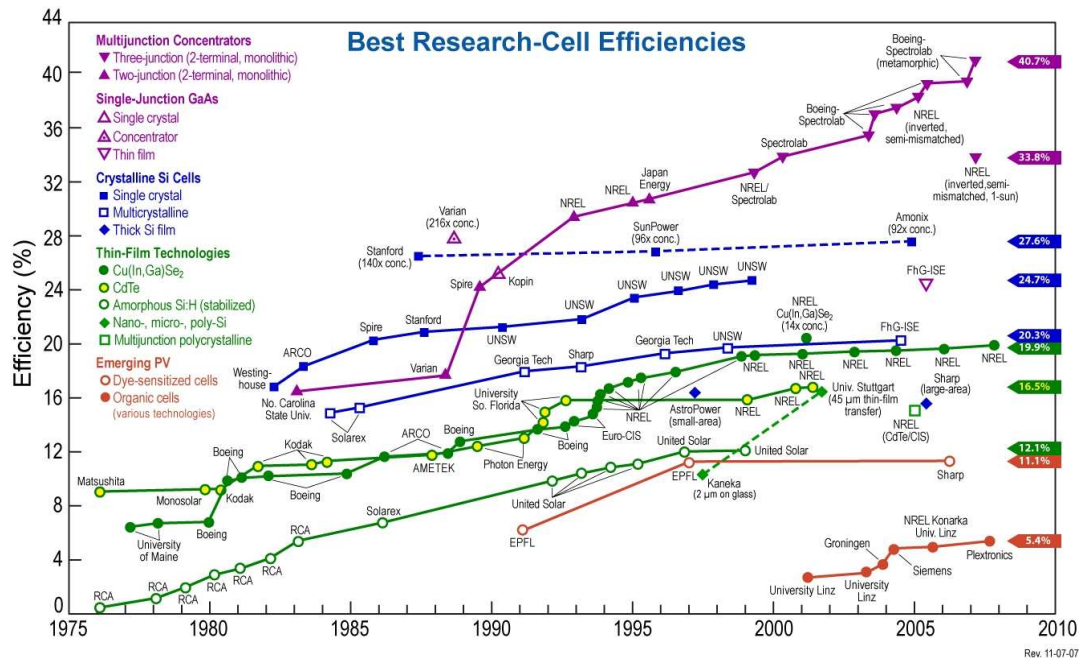
Figure 1.3 Best Research Cell Efficiencies [5].

II.   GENERATIONS OF SOLAR CELLS

Solar cells are categorized into three generations based on the order of their prominence. Research is being conducted on all the three generations concurrently to

improve their efficiencies while the first generation solar cells comprise the major share of commercial production about 89.7% in 2007 [6].

Large area, high quality and single junction devices form the 'first generation' solar cells. Reduction in production costs of this technology is nullified owing to high energy and labor costs, material costs mostly for the silicon wafer, strengthened low-iron glass cover sheet and costs of other encapsulants. This trend is continuing as the photovoltaic industry is expanding. Although it has a broad spectral absorption range, the high energy photons at the blue and violent end of the spectrum is wasted as heat [7]. Producing solar cells using high-efficiency processing sequences with high energy conversion efficiency are thus favored provided they do not increase the complexity of the solar cell. Theoretical limit on efficiency for single junction silicon solar cells i.e. 33% and this is also being reached very rapidly.
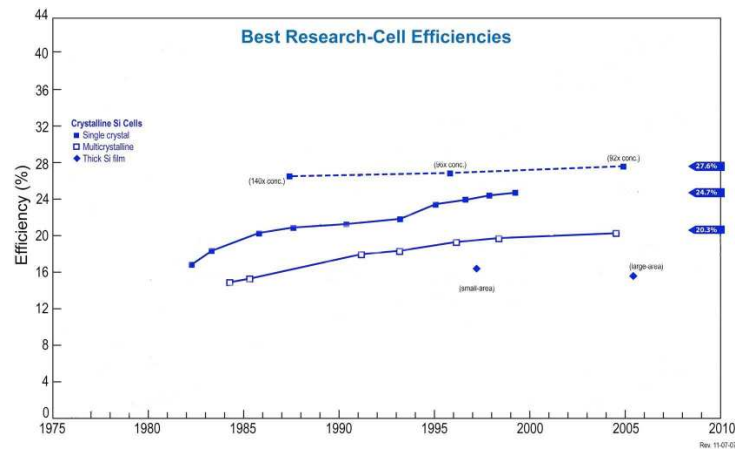
Figure 1.4 First Generation Solar Cell Efficiencies [7].

To address these problems of energy requirements and production costs of solar

cells a switch from 'first generation' to 'second generation' of thin-film cell technology has been imminent. By eliminating the silicon wafer a major reduction in material costs have been possible in the thin-film technology. They also have an advantage of increasing the unit size from silicon (~100cm^2) to glass plate (~1m^2). Over time the second generation solar cells are expected to bridge the gap between them and the first generation cells with respect to energy conversion efficiency. With the increase in dominance of this technology the costs of the constituent materials also goes up for top cover and other encapsulants to give it a longer life [8].

The materials generally used in this thin film technology are cadmium telluride, copper indium gallium arsenide, amorphous silicon and micromorphous silicon. These materials reduce mass and therefore cost by forming substrates for supporting glass and ceramics. Not only do they reduce costs but also promise very high energy conversion efficiency. A trend towards shifting to second generation from first generation is showing up but the commercialization of this technology has proven to be difficult [8]. Fortunately with the development of new materials over the coming decades the future of thin-film technology seems to be promising [6].

Research for improving solar cell performance by enhancing its efficiency and pushing it closer to the thermodynamic limits has led to the development of third generation solar cells [8]. To improve upon the poor electrical performance of the thin-film technology by maintaining low production costs this technology includes among others, non semiconductor technologies (including polymer based cells and biometrics) [9].
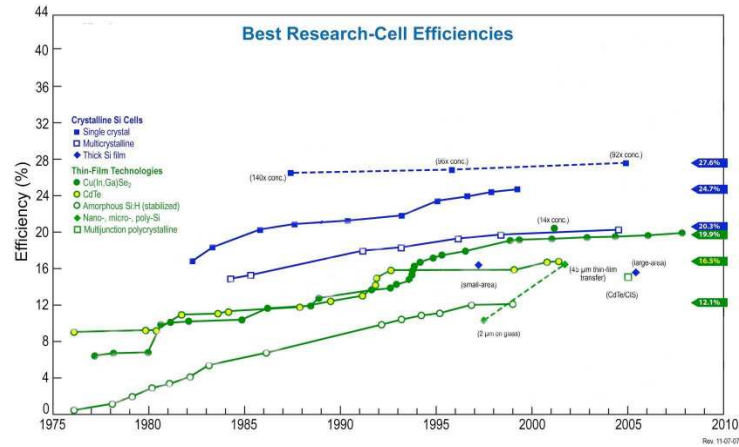
Figure 1.5 Second Generation Solar Cell Efficiencies [7]

The devices comprising the third generation solar cells are quantum dot technologies, tandem/multi junction cells, hot-carrier cells, up conversion technologies and solar thermal technologies like thermophotonics.
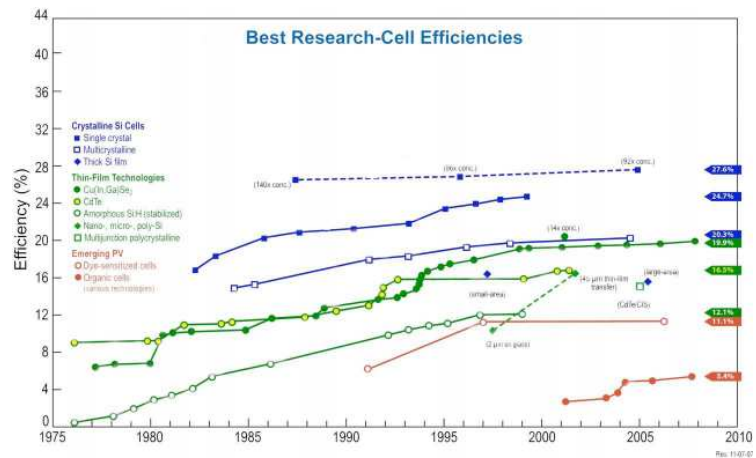
Figure 1.6 Third Generation Solar Cell Efficiencies [7].

III.   ULTIMATE LIMITS IN EFFICIENCY

The steady evolutionary progress of the PV industry is the result of increase in automation of production of thin film solar cells with increased efficiency and lower costs. The need for revolutionizing breakthroughs in the PV industry is sometimes halted by the advancements in the PV materials and manufacturing technology leading to improvements in the cost competitiveness and the expansion of the PV market. By shattering the old limits of efficiency and cost by bringing about innovations by exploiting new understanding of physics and material science will become a fast paced revolution [4].
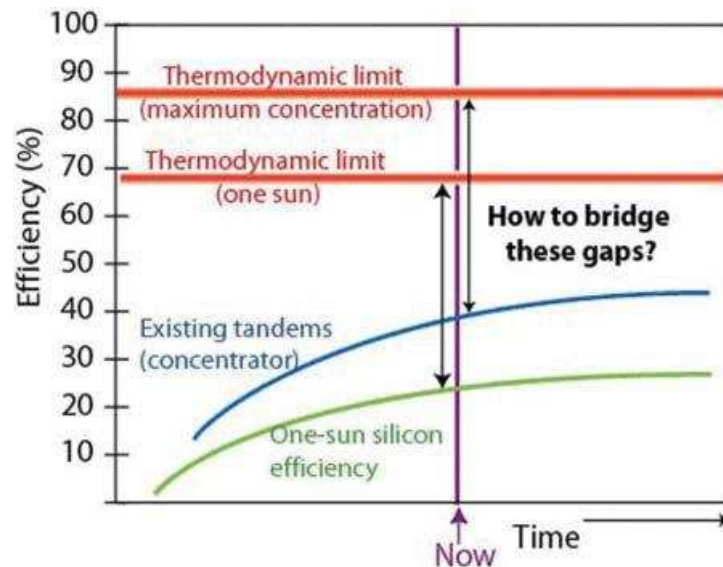
Figure 1.7 Narrowing gap between Existing and Theoretical PV efficiencies [4].

The maximum theoretical limit for a single junction solar cell without sunlight (one sun) is about 31% established by the Schokley-Quiesser limit. Under the highest possible amount of sunlight i.e. 50,000 suns a single junction solar cell can have a

maximum efficiency of about 41%. This efficiency value can be increased by using multi-junction solar cells by capturing more of the solar spectrum.

The true limit of efficiency is the thermodynamic limit of 68% for PV with one sun concentration and is about 87% for maximum solar concentration. Research and development in the PV industry are developing technologies based on concepts such as multiple exciton generation, optical frequency shifting, multi energy level and hot carrier devices. Carbon nanotubes, organic materials and other nanofabrication technologies enable these concepts in practice [4].

Approximate Theoretical Limit Efficiency		Approximate Best Experimental Performance to Date	
Thermodynamic (concentrator)	87%	n/a	
Thermodynamic (1 sun)	68%	n/a	
Six-junction	58%	n/a	
Hot carrier	54%	n/a	
Triple-junction concentrator	64%	44%	III-V alloys, monolithic stack
Triple-junction (1 sun)	49%	15%	Thin-film amorphous silicon alloys
Double-junction concentrator	56%	30%	III-V alloys, monolithic stack
Double-junction (1 sun)	43%	12%	Thin-film amorphous silicon alloys
Shockley-Queisser single-junction (46,200 suns)	41%	30%	Crystalline silicon (500 suns)
Shockley-Queisser single-junction (1 sun)	31%	24% 20% 12% 6%	Crystalline silicon Thin multicrystalline silicon Dye-sensitized cell Organic cell

Figure 1.8 Data showing potential magnitude of future improvements in performance across device configurations [4].

IV.   WORKING OF A SOLAR CELL
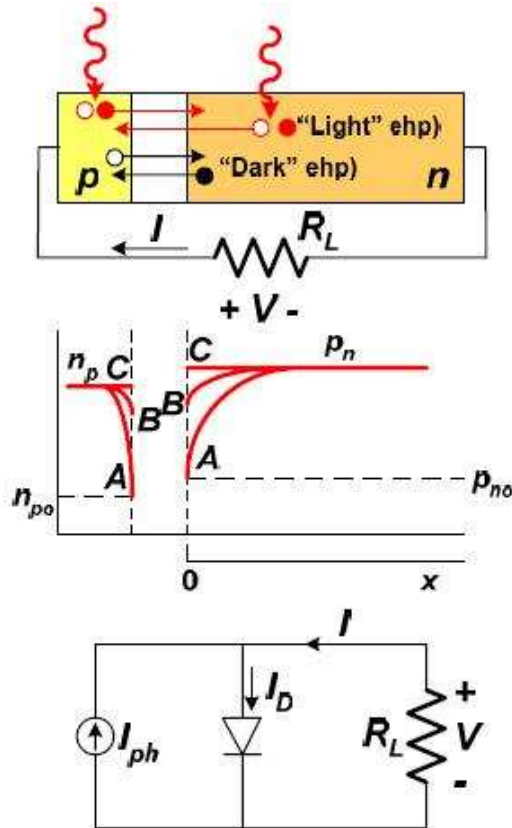
Figure 1.9 Working of a pn diode solar cell [10].

When light shines on a pn diode it generated electron-hole pairs across the whole device. If the device is open circuited, the electron hole pairs generated near the depletion region tend to recombine with the charge in the depletion region, thus reducing the depletion region charge and eventually reducing the depletion region. The reduction in depletion region is equivalent of applying a forward bias to the device i.e. this reduction in depletion region tends to develop a potential across the open terminals of the device. The maximum voltage that can be developed is the maximum forward drop across the

device which theoretically is possible with the complete elimination of the depletion region. This maximum voltage that can be developed across the open circuited device is called the open circuit voltage represented by the point C in Fig 1.9. If the device is short circuited, the generated holes and electrons produce a current corresponding to the incoming photons. This current is called the short circuit current represented by the point A in Fig 1.9. When the pn device is used to drive an external load say 'R' the region of operation is somewhere in between these two points. The reason being a current I flow through the device which creates a drop across the resistor and the direction of the current is such that the device comes into forward bias condition. As there is some drop across the load and the device the maximum output voltage is not equal to open circuit voltage. The forward bias conducts the device in the direction opposite to the current generated by the photons called the dark current. The presence of the dark current does not allow the device to operate at short circuit current. Thus the device operates in the fourth quadrant where the voltage is positive but the current is negative making the power negative i.e. the device generates power using light as source.
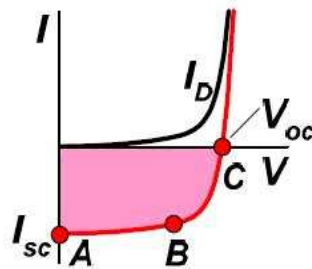
Figure 1.10 Current Voltage characteristics of solar cell [10].

V.   SOLAR CELL MODELLING HISTORY

The photovoltaic community has demonstrated and proposed a wide variety of solar cell structures using a wide range of photovoltaic semiconductor materials. Numerical modeling has proved to be a valuable tool in understanding the operation of these devices. There are several numerical solar cell simulation programs in use. The first solar cell program was developed by Mark S. Lundstrom as part of his PhD Thesis [11]. Other programs developed at Purdue University at later times include Thin-Film Semiconductor Simulation Program (TFSSP) [12], Solar Cell Analysis Program in 1 Dimension (SCAPlD), Solar Cell Analysis Program in 2 Dimension (SCAP2D) [13], PUPHS, and PUPHS2D [14]. These have been used to model a number of solar cells - thin-film Si:H, CdS/CIS, CdS/CdTe, Si, Ge, & GaAs cells in one spatial dimension and high efficiency Si and GaAs solar cells in two-dimensions.

One-dimensional simulations are usually adequate for conventional geometry solar cells, especially at low solar intensities and for semiconductor materials that are not well characterized. At high intensities, 2D effects can become important even in conventional geometry solar cells and many high efficiency cell designs require 2D simulations or even 3D simulations. The interdigitated back contact solar cell is an example of a 2D geometry and the point contact solar cell is an example of an inherently 3D geometry.

While the basic approach to modeling any of these devices is essentially the same, special purpose codes have typically been developed for each material. This usually

makes modification tedious since many different codes must be updated and tested. ADEPT (A Device Emulation Program and Toolbox) has been developed to address this problem by unifying the common components of all these codes [[12], [15]]. In addition, ADEPT was being developed to be a tool to examine novel materials and device structures.

Today, there are numerous solar cell programs developed by researchers from all over the world and there are also commercial simulation tools that can do solar cells modeling. Among those the best programs are probably Silvaco [16] and Crosslight [17], even though Synopsis has announced that it also has some solar cell simulation capabilities [18]. In SILVACO, TFT is an advanced device technology simulator equipped with the physical models and specialized numerical techniques required to simulate amorphous or polysilicon devices including thin film transistors. Specialized applications include the large area display electronics such as Flat Panel Displays (FPDs) and solar cells. In Crosslight, APSYS, Advanced Physical Models of Semiconductor Devices, is based on 2D/3D finite element analysis of electrical, optical and thermal properties of compound and silicon semiconductor devices. Emphasis has been placed on band structure engineering and quantum mechanical effects. Inclusion of various optical modules also makes this simulation package attractive for applications involving photosensitive or light emitting devices and solar cells. For Si rear-contacted cells (RCC) with textured front surface, RT techniques are utilized to compute the enhanced optic absorption. Conversion efficiency could be improved with about 20.7% percent for certain textured devices and good agreement with the experimental can be obtained.

Other Si cells, like passivated emitter, rear totally diffused (PERT), and passivated emitter, rear locally diffused (PERL) cells can also be modeled with APSYS. While EDA giant Synopsys Inc hasn't formally announced its solar cell simulation technology, the company discussed the capabilities of its Sentaurus technology as applied to solar cell design during the Semicon West tradeshow held in July, 2008.

VI.   PURPOSE AND CONTENT OF THIS THESIS

The purpose of this M.S. Thesis was to develop an in-house 3D drift-diffusion solar cell code that includes shadowing effects and utilize this code in the simulation of a prototypical Si solar cell. The existence of an in-house tool has the advantage that we can do modifications of the tool to include effects not covered in the above-described commercial simulation modules. Other purpose of this tool is to serve as a test-bed for the development of a Monte Carlo simulator for modeling solar cells that also includes the degradation in the solar cell efficiency due to lattice heating.

The thesis is organized as follows: In Chapter 2 we describe in details the theoretical model implemented in the simulator and the numerical methods used for the solution of the 3D Poisson and the 3D electron and hole continuity equations. In Chapter 3 the results of the structures simulated have been presented. The I-V plots, Carrier density distributions, Potential profiles, Electric field profiles, effect of Shadowing, efficiency variation with the length of the device has been presented. In the final Chapter i.e. Chapter 4 the summary and future work haven been stated.

Chapter 2

DRIFT DIFFUSION MODELING

I.   DRIFT DIFFUSION MODEL

The semi classical transport of charges can be explained using BTE (Boltzmann Transport equation). However, the direct analytical solution of the BTE is difficult combined with the field solvers for device simulation. Therefore the predominant model providing solutions for the Drift Diffusion equations is generally used for traditional semiconductor device modeling. In this model the electric fields and spatial gradient of the carrier density is localized i.e. the current at a particular point only depends on the instantaneous electric field and concentration gradient of carriers at that point.

The drift diffusion equations can be obtained by solving the BTE (Boltzmann Transport equation) by solving for the moments of this equation. For steady-state and 1D geometry, the use of relaxation time approximation for the BTE results in

$$\frac{eE}{m^*}\frac{\partial f}{\partial v} + v\frac{\partial f}{\partial v} = \frac{f_0 - f(v,x)}{\tau} \tag{2.1}$$

The assumption of parabolic bands has been considered for simplicity. The current density is defined as,

$$J(x) = e\int vf(v,x)dv \tag{2.2}$$

Here, the integral on the right –hand side represents the first moment of the distribution function. By multiplying eq. (2.1) by v on both sides and integrating over v we can relate it to the definition of the current. We thus obtain,

$$\frac{1}{\tau}\left[\int vf_0 dv - \int vf(v,x)dv\right] = -\frac{J(x)}{e\tau} \tag{2.3}$$

Since the equilibrium distribution function is symmetric in v, the first integral goes to zero. Therefore, we have

$$J(x) = -e\tau\left[\frac{eE}{m*}\int v\frac{\partial f}{\partial v}dv - \frac{d}{dx}\int v^2 f(v,x)dv\right] \tag{2.4}$$

Integrating the above equation by parts we get,

$$\int v\frac{\partial f}{\partial v}dv = [vf(v,x)]_{-\infty}^{\infty} - \int f(v,x)dv = -n(x) \tag{2.5}$$

The above equation can be written as,

$$\int v^2 f(v,x)dv = n(x)\langle v^2 \rangle \tag{2.6}$$

Here, $\langle v^2 \rangle$ represents the average of the square of the velocity. By introducing mobility $\mu = e\tau/m*$ and assuming that most of the average carrier energy (that is proportional to $\langle v^2 \rangle$) is due to the random thermal motion of the carriers we can replace this term with its equilibrium value i.e. $k_B T/m*$ in 1D case and $3k_B T/m*$ for 3D. By introducing the Diffusion coefficient D we obtain the drift diffusion equations as,

$$J_n = qn(x)\mu_n E(x) + qD_n \frac{dn}{dx}$$

$$J_p = qp(x)\mu_p E(x) - qD_p \frac{dp}{dx} \tag{2.7}$$

Even though no assumptions were made for the non-equilibrium distribution function $f(v,x)$ the choice of the thermal velocity signifies that the-drift diffusion equations are only valid for small perturbations from the equilibrium state (low fields).

Numerical schemes involving solution of the continuity equations follow the rules that the total charge inside the device as well as the charge leaving and entering the device must be considered. Carrier density localized in a place has to be positive i.e. negative density is unphysical. Also, no spurious space oscillations have to be introduced i.e. monotonicity of the solution has to be maintained [19]. The complete drift-diffusion model, which includes the Poisson Equation and the continuity equations for electrons and holes is given below:

II.   SCHARFETTER GUMMEL DISCRETIZATION OF CONTINUITY EQUATIONS

A. *Discretization of the Continuity Equation*

Generally, conservative schemes are achieved by subdivision of the computational domain into boxes surrounding the mesh points. Currents are defined on

the boundaries of these elements, thus enforcing conservation. Consider the 1D electron current continuity equation under steady state equations:

$$\frac{1}{e}\nabla.J_n = G \tag{2.8}$$

which by using half-point difference expansion based on the centered difference scheme, gives:

$$\frac{1}{e}(\frac{J_{i+1/2}^n - J_{i-1/2}^n}{\Delta}) = G_i \tag{2.9}$$

where,

$$J_{i+1/2}^n = en\mu_{i+1/2}^n E_{i+1/2} + eD_{i+1/2}^n \frac{dn}{dx} \tag{2.10}$$

$$\frac{dn}{dx} + \frac{n\mu_{i+1/2}^n E_{i+1/2}}{D_{i+1/2}^n} = \frac{J_{i+1/2}^n}{eD_{i+1/2}^n} \tag{2.11}$$

$$\frac{dn}{dx} - \frac{n\mu_{i+1/2}^n E_{i+1/2}}{V_t} = \frac{J_{i+1/2}^n}{eD_{i+1/2}^n} \tag{2.12}$$

We make use of the following,

$$\frac{dn}{dx} = \frac{dn}{d\Psi}\frac{d\Psi}{dx} = \frac{dn}{d\Psi}\frac{\Psi_{i+1} - \Psi_i}{\Delta} \tag{2.13}$$

to get,

$$\frac{dn}{d\Psi} - \frac{n}{V_t} = \frac{\Delta}{e(\Psi_{i+1} - \Psi_i)} \frac{J_{i+1/2}^n}{D_{i+1/2}^n}$$ (2.14)

Using Laplace transform and the conditions,

$$n(\Psi_i) = n_i \qquad n(\Psi_{i+1}) = n_{i+1}$$ (2.15)

We get,

$$n(\Psi) = n_i[1 - g(\Psi)] + n_{i+1}g(\Psi)$$ (2.16)

where, $$g(\Psi) = \frac{e^{\frac{\Psi - \Psi_i}{V_t}} - 1}{e^{\frac{\Psi_{i+1} - \Psi_i}{V_t}} - 1}$$ (2.17)

Therefore,

$$J_{i+1/2}^n = \frac{eD_{i+1/2}^n}{\Delta}[n_{i+1}B(\frac{\Psi_{i+1} - \Psi_i}{V_t}) - n_i B(\frac{\Psi_i - \Psi_{i+1}}{V_t})]$$ (2.18)

In the above equation $B(x)$ is Bernoulli function, $B(x) = \dfrac{x}{e^x - 1}$

Similarly,

$$J_{i-1/2}^n = \frac{eD_{i-1/2}^n}{\Delta}[n_i B(\frac{\Psi_i - \Psi_{i-1}}{V_t}) - n_{i-1}B(\frac{\Psi_{i-1} - \Psi_i}{V_t})]$$ (2.19)

The equations (2.18) and (2.19) represent the discretization of the current density expressions that can be used to calculate the total current in the device. Thus, the discretized form of continuity equations for electrons and holes respectively is,

$$
\frac{D_{i+1/2}^{n}}{\Delta^2} B(\frac{\Psi_{i+1} - \Psi_i}{V_t})n_{i+1} - n_i[\frac{D_{i-1/2}^{n}}{\Delta^2} B(\frac{\Psi_i - \Psi_{i-1}}{V_t}) + \frac{D_{i+1/2}^{n}}{\Delta^2} B(\frac{\Psi_i - \Psi_{i+1}}{V_t})]
$$
$$
+ \frac{D_{i-1/2}^{n}}{\Delta^2} B(\frac{\Psi_{i-1} - \Psi_i}{V_t})n_{i-1} = G_i \tag{2.20}
$$

$$
\frac{D_{i-1/2}^{p}}{\Delta^2} B(\frac{\Psi_i - \Psi_{i-1}}{V_t})p_{i-1} - p_i[\frac{D_{i-1/2}^{p}}{\Delta^2} B(\frac{\Psi_{i-1} - \Psi_i}{V_t}) + \frac{D_{i+1/2}^{p}}{\Delta^2} B(\frac{\Psi_{i+1} - \Psi_i}{V_t})]
$$
$$
+ \frac{D_{i+1/2}^{p}}{\Delta^2} B(\frac{\Psi_i - \Psi_{i+1}}{V_t})p_{i+1} = G_i \tag{2.21}
$$

Scharfetter-Gummel scheme leads to positive definitive matrices eliminating the occurrence of complex Eigen valued coefficient matrices. Therefore the SOR (Successive over relaxation method) can be used as a numerical computation method. Linear interpolation schemes can be used in determining the half point values for the diffusion coefficient and carrier mobility,

$$
D_{i+1/2} = \frac{D_i + D_{i+1}}{2} \qquad \mu_{i+1/2} = \frac{\mu_i + \mu_{i+1}}{2} \tag{2.22}
$$

Bernoulli function can be defined in the following way,

$$B(x) = \begin{cases} -x, x < x_1 \\ \dfrac{x}{e^x - 1}, x_1 \le x < x_2 \\ 1 - \dfrac{x}{2}, x_2 \le x < x_3 \\ \dfrac{xe^{-x}}{1 - e^{-x}}, x_3 \le x \le x_4 \\ xe^{-x}, x_4 \le x < x_5 \\ 0, x \ge x_5 \end{cases} \tag{2.23}$$

where, x_1 through x_5 depend upon the computer [20].

B. *Numerical Solution of Continuity equation using Bi-Conjugate gradient stabilized method*

Conjugate gradient methods are very effective to solve large system of linear equations. The equations of the type,

$$Ax = b \tag{2.24}$$

where x is an unknown vector, b is a known vector and A is a known square, symmetric, positive definite matrix (or positive indefinite matrix). Many numerical systems involving finite difference and finite element methods adopt this method to solve set of partial difference equations. These methods are generally used with sparse matrices. Dense matrices are very hard to solve as they have to be factorized which would take the same time as to solve it iteratively. Factorizing requires a lot of memory and it is much slower than the iterative methods. By the use of sparse matrices the efficiency and the memory utilization of the numerical methods improves [21].

This algorithm is used for a function of n variables for finding its local minimum under the assumption that the gradient of the function can be computed. Conjugate directions is used instead of local gradient for going downhill unlike steepest decent method and if the vicinity of the minimum is in the shape of a long narrow valley convergence is achieved much faster than the steepest decent method. It is the oldest and best known non stationary method for solving positive definite systems effectively.

Vector sequences of iterations which are successive approximations to the solution are generated, residues corresponding to these iterations are computed and directions used in updating these residues and iterations are searched for. The memory utilized by this algorithm is less since only a small number of sequences are required to be stored although the length of these vectors is large. In order to compute update scalars that are defined to make the sequences satisfy certain orthogonality conditions two inner products are performed for every iteration in this method. These conditions imply that the distance to the true solution is minimized on a positive definitive linear system.

The search direction vector $p^{(i)}$ is found by updating the iterates $x^{(i)}$ in every iteration by a multiple α_i ,

$$x^{(i)} = x^{(i-1)} + \alpha_i p^{(i)} \tag{2.25}$$

The residuals $r^{(i)} = b - Ax^{(i)}$ are updated as,

$$r^{(i)} = r^{(i-1)} - \alpha_i q^{(i)} \tag{2.26}$$

where,

$$q^{(i)} = Ap^{(i)} \tag{2.27}$$

The proper choice of α i.e. $\alpha_i = \dfrac{r^{(i-1)^T} r^{(i-1)}}{p^{(i)^T} Ap^{(i)}}$ minimizes $r^{(i)^T} A^{-1} r^{(i)}$ over all possible

choices of α. The residuals used in updating the search vectors are,

$$p^{(i)} = r^{(i)} + \beta_{i-1} p^{(i-1)} \tag{2.28}$$

where,

$$\beta_i = \dfrac{r^{(i)^T} r^{(i)}}{r^{(i-1)^T} r^{(i-1)}} \tag{2.29}$$

This choice of β_i is done to ensure that $p^{(i)}$ and $Ap^{(i-1)}$ i.e. the residuals $r^{(i)^T}$ and $r^{(i-1)}$

are orthogonal. It also makes $p^{(i)}$ and $r^{(i)^T}$ orthogonal to all previous $Ap^{(j)}$ and $r^{(j)^T}$

respectively. This algorithm is not preconditioned. The preconditioned form of Conjugate

gradient method is done by using a preconditioner M (when M = 1 it is without

preconditioning). Thus, the pseudocode for preconditioned conjugate gradient method is,

Compute $r^{(0)} = b - Ax^{(0)}$ for some initial guess $x^{(0)}$. For every value of i we

solve for $Mz^{(i-1)} = r^{(i-1)}$ and we have $\rho_{i-1} = r^{(i-1)^T} z^{(i-1)}$. The value of $p^{(i)}$ is,

$$p^{(1)} = z^{(0)} \text{ (If } i = 1 \text{)} \qquad \text{else} \quad p^{(i)} = z^{(i-1)} + \beta_{i-1} p^{(i-1)} \quad \text{where,}$$

$$\beta_{i-1} = \frac{\rho_{i-1}}{\rho_{i-2}}$$

The values of $q^{(i)}$, α_i, $x^{(i)}$ and $r^{(i)}$ are updated till convergence is reached.

$$q^{(i)} = A p^{(i)}$$

$$\alpha_i = \frac{\rho_{i-1}}{p^{(i)^T} q^{(i)}}$$

$$x^{(i)} = x^{(i-1)} + \alpha_i p^{(i)} \qquad r^{(i)} = r^{(i-1)} - \alpha_i q^{(i)}$$

Conjugate gradient method has one matrix vector product, two inner products and three vector updates per iteration. This makes it computationally very attractive [22].

The residual vectors for non symmetric systems cannot be made orthogonal and therefore conjugate gradient method cannot be used to solve such systems. The orthogonality of the residues can be maintained by using long sequences as per the generalized minimal residual method but at the cost of lot of storage space. Another approach can be followed by using two mutually orthogonal sequences instead of the orthogonal sequences of residuals called the Bi conjugate gradient Method (BCG).The update sequences of the two residuals are,

$$r^{(i)} = r^{(i-1)} - \alpha_i A p^{(i)} \qquad\qquad r^{\sim(i)} = r^{\sim(i-1)} - \alpha_i A^T p^{\sim(i)} \qquad\qquad (2.30)$$

and the two search direction vectors are,

$$p^{(i)} = r^{(i-1)} + \beta_{i-1} p^{(i-1)} \qquad\qquad p^{\sim(i)} = r^{\sim(i-1)} + \beta_{i-1} p^{\sim(i-1)} \qquad\qquad (2.31)$$

The choices are,

$$\alpha_i = \frac{r^{\sim(i-1)^T} r^{(i-1)}}{p^{\sim(i)^T} A p^{(i)}} \qquad\qquad \beta_i = \frac{r^{\sim(i)^T} r^{(i)}}{r^{\sim(i-1)^T} r^{(i-1)}} \qquad\qquad (2.32)$$

ensuring orthogonality relations,

$$r^{\sim(i)^T} r^{(j)} = p^{\sim(i)^T} A p^{(j)} = 0 \qquad\qquad (2.33)$$

Thus we observe that updates for the residuals in conjugate gradient method are augmented in the bi-conjugate gradient method by the relations that are similar but based on A^T instead of A [22].

The algorithm for BCG method is, (if $i \ne j$)

Compute $r^{(0)} = b - Ax^{(0)}$ for some initial guess $x^{(0)}$. Choose $r^{\sim(0)}$ (for example $r^{\sim(0)} = r^{(0)}$). For every value of i we solve for $Mz^{(i-1)} = r^{(i-1)}$ and $M^T z^{\sim(i-1)} = r^{\sim(i-1)}$. We also have $\rho_{i-1} = z^{(i-1)^T} r^{\sim(i-1)}$. If $\rho_{i-1} = 0$ then the method fails. The value of $p^{(i)}$ and $p^{\sim(i)}$ are,

$$p^{(i)} = z^{(i-1)} \qquad\qquad p^{\sim(i)} = z^{\sim(i-1)} \text{ (If } i = 1)$$

else $\qquad\qquad p^{(i)} = z^{(i-1)} + \beta_{i-1} p^{(i-1)} \qquad\qquad p^{\sim(i)} = z^{\sim(i-1)} + \beta_{i-1} p^{\sim(i-1)} \qquad$ where,

$$\beta_{i-1} = \frac{\rho_{i-1}}{\rho_{i-2}}$$

The values of $q^{(i)}, q^{\sim(i)}, \alpha_i, x^{(i)}, r^{(i)}$ and $r^{\sim(i)}$ are updated till convergence is reached as,

$$q^{(i)} = Ap^{(i)} \qquad\qquad q^{\sim(i)} = A^T p^{\sim(i)}$$

$$\alpha_i = \frac{\rho_{i-1}}{p^{(i)^T} q^{(i)}}$$

$$x^{(i)} = x^{(i-1)} + \alpha_i p^{(i)}$$

$$r^{(i)} = r^{(i-1)} - \alpha_i q^{(i)} \qquad\qquad r^{\sim(i)} = r^{\sim(i-1)} - \alpha_i q^{\sim(i)}$$

The above algorithm when used for positive definite symmetric matrices gives the same result as the conjugate gradient stabilized method but at twice the cost per iteration. For non symmetric matrices this method is more or less similar to the generalized minimal residue method although a significant reduction in the norm of the residual is observed.

To avoid the irregular pattern in the convergence of the conjugate gradient squared method the Bi-conjugate gradient stabilized method was developed. Instead of computing the conjugate gradient squared method sequence $i \rightarrow P_i^2(A)r^{(0)}$, BCGSTAB uses $i \rightarrow Q_i(A)P_i(A)r^{(0)}$ where Q is an ith degree polynomial describing the steepest decent update. This algorithm requires two-matrix vector products, four inner products

which is two more than the conjugate gradient squared method or the bi-conjugate gradient method. The algorithm is [22],

Compute $r^{(0)} = b - Ax^{(0)}$ for some initial guess $x^{(0)}$. Choose $r^{\sim(0)}$ (for example $r^{\sim(0)} = r^{(0)}$). For every value of i we calculate $\rho_{i-1} = r^{\sim T} r^{(i-1)}$. If $\rho_{i-1} = 0$ then the method fails. The value of $p^{(i)}$ is,

$$p^{(i)} = r^{(i-1)} \ (\text{If } i = 1) \qquad \text{else} \quad p^{(i)} = r^{(i-1)} + \beta_{i-1}(p^{(i-1)} - \omega_{i-1}v^{(i-1)}) \quad \text{where,}$$

$$\beta_{i-1} = (\frac{\rho_{i-1}}{\rho_{i-2}})(\frac{\alpha_{i-1}}{\omega_{i-1}})$$

We solve for $Mp^{\sim} = p^{(i)}$. The values of α_i and s are given by,

$$\alpha_i = \frac{\rho_{i-1}}{r^{\sim T}v^{(i)}} \qquad\qquad s = r^{(i-1)} - \alpha_i v^{(i)}$$

We check norm of s; if small enough: set $x^{(i)} = x^{(i-1)} + \alpha_i p^{\sim}$ and stop. We then solve for $Ms^{\sim} = s$. We update t, ω_i, $x^{(i)}$ and $r^{(i)}$ till convergence is achieved,

$$t = As^{\sim}$$

$$\omega_i = \frac{t^T s}{t^T t}$$

$$x^{(i)} = x^{(i-1)} + \alpha_i p^{\sim} + \omega_i s^{\sim}$$

$$r^{(i)} = s - \omega_i t$$

III.   POISSON EQUATION SOLVER

A. Discretization of the 3D Poisson Equation

The potential variation in a semiconductor device can be determined by solving the Poisson equation,

$$\nabla(\varepsilon.\nabla\psi) = \rho = q(n - p + N_A^- - N_D^+) \tag{2.24}$$

where ε is the dielectric constant of the corresponding semiconductor, ψ is the electrostatic potential, ρ is the total charge density, q is the elementary charge, n is the electron concentration, p represents the hole concentration, N_A^- is the ionized acceptor concentration and N_D^+ is the ionized donor concentration.

The electron and hole densities at thermal equilibrium for non degenerate materials is given by,

$$n = n_i e^{(\frac{E_F - E_i}{k_B T})} \qquad\qquad p = p_i e^{(\frac{E_i - E_F}{k_B T})} \tag{2.25}$$

where n and p represent the electron and hole concentration respectively, n_i is the intrinsic carrier concentration, E_F is the Fermi Energy level and E_i the intrinsic energy level. Taking $E_F = 0$ i.e. the Fermi energy level being the reference and representing Energy in terms of potential i.e. $E_i = -q\psi$ we get,

$$n = n_i e^{\phi} \qquad\qquad p = p_i e^{-\phi} \tag{2.26}$$

Here ψ represents the potential, ϕ represents the normalized potential i.e. ψ is normalized with the thermal voltage $V_T = k_B T / q$. Assuming the device is made of the same material i.e. no variation in ε, Poisson equation can be represented as

$$\nabla^2 \phi = \frac{q n_i}{V_T \varepsilon} (e^{\phi} + e^{-\phi} + C') \tag{2.27}$$

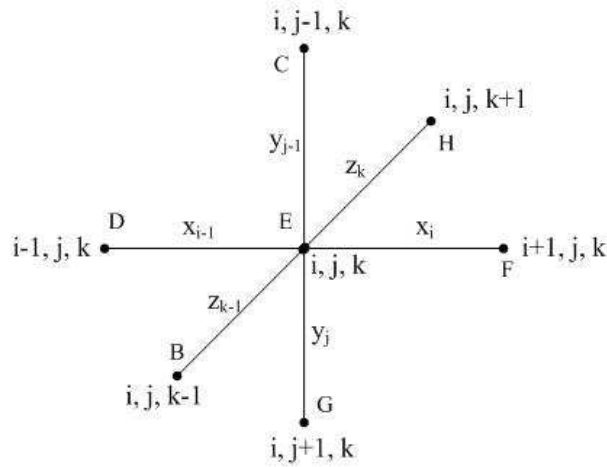where the normalized dopant concentration is represented by C' and $C' = (N_A^- - N_D^+)/n_i$

Figure 2.1 Central difference scheme in 3D leading to a 7-point discretization stencil

Expressing the second derivative of the potential in the Poisson equation using the Central difference scheme as shown in Figure 2.1 in all the three directions we obtain,

$$\frac{\partial^2 \phi_{i,j,k}}{\partial x^2} = \frac{2\phi_{i+1,j,k}}{x_i(x_i + x_{i-1})} - \frac{2\phi_{i,j,k}}{x_i x_{i-1}} + \frac{2\phi_{i-1,j,k}}{x_{i-1}(x_i + x_{i-1})} \tag{2.28}$$

$$\frac{\partial^2 \phi_{i,j,k}}{\partial y^2} = \frac{2\phi_{i,j+1,k}}{y_j(y_j + y_{j-1})} - \frac{2\phi_{i,j,k}}{y_j y_{j-1}} + \frac{2\phi_{i,j-1,k}}{y_{j-1}(y_j + y_{j-1})}, \text{ and} \qquad (2.29)$$

$$\frac{\partial^2 \phi_{i,j,k}}{\partial z^2} = \frac{2\phi_{i,j,k+1}}{z_k(z_k + z_{k-1})} - \frac{2\phi_{i,j,k}}{z_k z_{k-1}} + \frac{2\phi_{i,j,k-1}}{z_{k-1}(z_k + z_{k-1})} \qquad (2.30)$$

By combining all these three equations we can get the expression for $\nabla^2 \phi$. The mesh sizes along the x, y and z direction are given by x_i, y_j and z_k, respectively, as shown in Figure 2.1. Thus the finite-difference representation of the 3D Poisson equation is given by,

$$\frac{\phi_{i+1,j,k} - \phi_{i,j,k}}{x_i(x_i + x_{i-1})} + \frac{\phi_{i-1,j,k} - \phi_{i,j,k}}{x_{i-1}(x_i + x_{i-1})} + \frac{\phi_{i,j+1,k} - \phi_{i,j,k}}{y_j(y_j + y_{j-1})} + \frac{\phi_{i,j-1,k} - \phi_{i,j,k}}{y_{j-1}(y_j + y_{j-1})} +$$

$$+ \frac{\phi_{i,j,k+1} - \phi_{i,j,k}}{z_k(z_k + z_{k-1})} + \frac{\phi_{i,j,k-1} - \phi_{i,j,k}}{z_{k-1}(z_k + z_{k-1})} = \frac{1}{2L_D^2}(C'_{i,j,k} + n_{i,j,k} - p_{i,j,k}) \qquad (2.31)$$

where the intrinsic Debye length, $L_D = \sqrt{V_T \varepsilon / (qn_i)}$. The carrier concentrations n and p are normalized by the intrinsic concentration, n_i as given by Equation (2.31). The above equation can also be represented as,

$$B_{i,j,k}\phi_{i,j,k-1} + C_{i,j,k}\phi_{i,j-1,k} + D_{i,j,k}\phi_{i-1,j,k} + E_{i,j,k}\phi_{i,j,k} +$$

$$+ F_{i,j,k}\phi_{i+1,j,k} + G_{i,j,k}\phi_{i,j+1,k} + H_{i,j,k}\phi_{i,j,k+1} = Q_{i,j,k} \qquad (2.32)$$

where

$$B_{i,j,k} = \frac{2}{z_{k-1}(z_k + z_{k-1})} \qquad\qquad C_{i,j,k} = \frac{2}{y_{j-1}(y_j + y_{j-1})}$$

$$D_{i,j,k} = \frac{2}{x_{i-1}(x_i + x_{i-1})} \qquad\qquad F_{i,j,k} = \frac{2}{x_i(x_i + x_{i-1})} \qquad (2.33)$$

$$G_{i,j,k} = \frac{2}{y_j(y_j + y_{j-1})} \qquad\qquad H_{i,j,k} = \frac{2}{z_k(z_k + z_{k-1})} ,$$

$$E_{i,j,k} = -\left(\frac{2}{x_i x_{i-1}} + \frac{2}{y_j y_{j-1}} + \frac{2}{z_k z_{k-1}} \right) \qquad Q_{i,j,k} = \left(C'_{i,j,k} + n_{i,j,k} - p_{i,j,k} \right)$$

It is important to note that all the discretization increments x_i, y_j and z_k appearing in Eq. (3.10), are normalized with the intrinsic Debye length L_D. Charge neutrality condition is used to calculate the initial concentration for n and p for a good initial guess for potential in the RHS of equation (2.32).

B. Linearization of the Discretized 3D Poisson Equation

A matrix equation $Ax=b$ is formed when the Poisson equation of the form as represented in equation (2.32) is solved for the entire device divided into nodes. Here A is the discretization matrix, x is the unknown potential and b is the forcing function, also called the forcing vector (charge, in the case of Poisson equation). This form of the equation cannot be directly used to numerically solve for the potential profile in the device as it leads to instabilities since the RHS of the equation (2.32) has an exponential relation to the potential ϕ through the carrier concentrations n and p. The center

coefficient E is not diagonally dominant as compared to the other coefficients B, C, D, F, G and H in the matrix A. Fast convergence demands the matrix to be diagonally dominant i.e. the coefficient on the diagonal is larger than the sum of the other non diagonal elements. In order to achieve diagonal dominance for the coefficient matrix A Poisson equation has to be linearised. To achieve the above the first update of the potential is defined as [23]

$$\phi^{n+1} = \phi^n + \delta^n \tag{2.34}$$

where the potential in the next update is ϕ^{n+1} and is calculated by using the potential from the previous iteration ϕ^n and a correction factor δ^n. By substituting the above variables in the Poisson equation we get,

$$\nabla^2 \phi^{n+1} = \frac{1}{L_D^2} \left(e^{\phi^n + \delta^n} - e^{-\phi^n - \delta^n} + C' \right) \tag{2.35}$$

Assuming the update of potential between iterations being small i.e. for small δ Taylor's series can be used for the exponential function $e^{\pm \delta} = 1 \pm \delta$. Thus the Poisson equation becomes,

$$\nabla^2 \phi^{n+1} = \frac{1}{L_D^2} \left(e^{\phi^n} - e^{-\phi^n} + C' \right) + \frac{1}{L_D^2} \left(e^{\phi^n} - e^{-\phi^n} \right) \delta^n \tag{2.36}$$

By replacing δ^n in equation (2.36) with ϕ^{n+1} and ϕ^n by using equation (2.34) we obtain,

$$\nabla^2 \phi^{n+1} - \frac{1}{L_D^2} \left(e^{\phi^n} - e^{-\phi^n} \right) \phi^{n+1} = \frac{1}{L_D^2} \left(e^{\phi^n} - e^{-\phi^n} + C' \right) - \frac{1}{L_D^2} \left(e^{\phi^n} - e^{-\phi^n} \right) \phi^n \tag{2.37}$$

In the above equation index n represents the iteration number and not the node number. By using central difference scheme equation (2.37) can be expressed in terms of equation (2.32). The center coefficient E and the forcing function Q can be expressed as [24],

$$E_{i,j,k} = -\left(\frac{2}{x_i x_{i-1}} + \frac{2}{y_j y_{j-1}} + \frac{2}{z_k z_{k-1}} \right) - \frac{1}{L_D^{\,2}} \left(n_{i,j,k} + p_{i,j,k} \right)$$

$$Q_{i,j,k} = \left(C_{i,j,k}' + n_{i,j,k} - p_{i,j,k} \right) - \frac{1}{L_D^{\,2}} \left(n_{i,j,k} + p_{i,j,k} \right) \phi_{i,j,k} \qquad (2.38)$$

To make the center coefficient diagonally dominant and increase the speed and stability of the convergence the linearization of Poisson equation is done. In addition the center coefficient is now dependent on the electron and hole carrier concentrations, thus have to be updated for every iteration. ϕ_A

C. Boundary Conditions

Ohmic and artificial contacts in the device structure can be described by making modifications to the coefficients B through H, and the forcing function Q. These modifications are,

- *Ohmic contacts* are implemented by fixing the potential at these points equal to the sum of the external bias applied ϕ_A and the potential due to charge neutrality V_b. This is called Dirichlet condition and is implemented as,

$$\phi = \phi_A + V_b, \tag{2.39}$$

$$B = C = D = F = G = H = 0, \ E = 1 \quad \text{and} \, Q = \phi_A + V_b. \tag{2.40}$$

- Simulation domain is fixed in size and therefore has to be truncated. This can be done by using artificial boundaries and the boundary condition enforced is called Neumann condition. It is implemented by making the field across the boundary equal to zero i.e.,

$$\frac{\partial \phi}{\partial \vec{r}} = 0. \tag{2.41}$$

Using central difference scheme equation (2.41) can be written as,

$$\frac{\phi_{i+1} - \phi_{i-1}}{x_i} = 0 \quad \text{or} \quad \phi_{i+1} = \phi_{i-1}, \tag{2.42}$$

The same concept is also used for the other directions. Using equation (2.42) in the discretization of the coefficients B through H we obtain,

$$z = 0 \ : \ B = 0, \ H = 2H, \qquad\qquad z = z_{\max} : \ B = 2B, \ H = 0,$$

$$y = 0 \ : \ C = 0, \ G = 2G, \qquad\qquad y = y_{\max} : \ C = 2C, \ G = 0, \tag{2.43}$$

$$x = 0 \ : \ D = 0, \ F = 2F, \qquad\qquad x = x_{\max} : \ D = 2D, \ F = 0.$$

Chapter 3

SIMULATION RESULTS

The theory behind the simulation of the solar cells and the corresponding models used was explained in Chapter 2. The self consistent solution of the Poisson and continuity equations is used to simulate the potential and carrier profiles in the device. By extracting the current densities from the simulation, open circuit voltage and short circuit current can be evaluated to find the efficiency of the silicon solar cell.

The following Chapter is divided broadly into four parts; first part explains the silicon solar cell structures simulated and the inputs regarding the solar radiation and absorption coefficients of the material, second part presents the simulation results for these structures under illumination without any shadowing or surface recombination effects i.e. assuming transparent contacts, third part of the chapter deals with the simulation of these structures with shadowing and surface recombination effects and the final part explains the methodology adapted in calculation of efficiency and the plots for the trends in efficiency with the variation in structure dimensions is presented.

I.   STRUCTURES SIMULATED AND INPUTS USED FOR THE SIMULATION

Initially to inspect the effectiveness of drift-diffusion modeling for solar cells a 1D simulation for a p-n junction silicon solar cell was performed. It is a single junction with uniformly doped layers and a single sun radiation is utilized as the energy source for the device. The device is simulated with the assumption of transparent contact i.e. no shadowing and surface recombination.
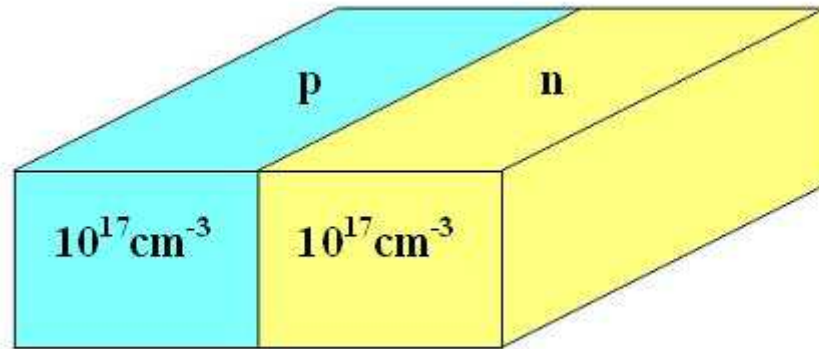
Figure 3.1 p-n junction Silicon Solar Cell

The solar radiation which is used in this simulation is the ASTM G173-03 Reference spectra derived from SMARTS v. 2.9.2 for AM1.5 one sun. The solar spectrum used is,
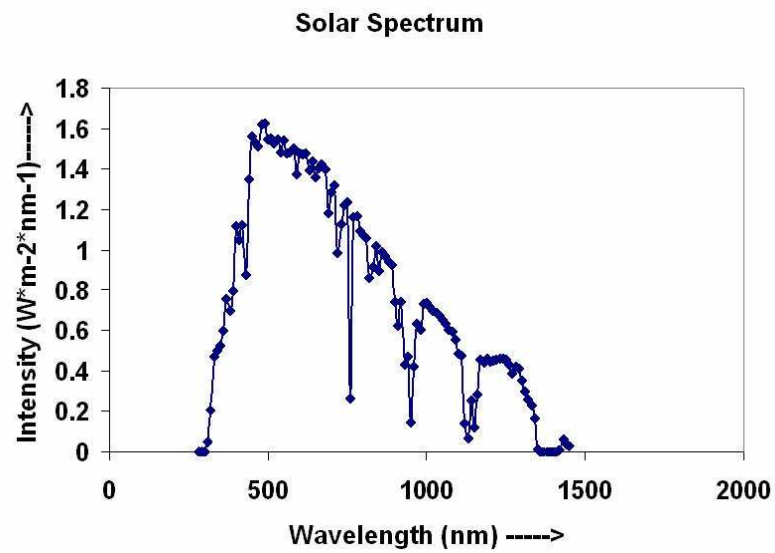

Figure 3.2 Solar spectrum for AM 1.5

The solar spectrum in Figure 3.2 is used to input the Photon Intensity into the simulation which is utilized to calculate the number of carrier contribution by individual wavelengths in the solar cell. The other parameter which is required to find out the effective number of photons absorbed i.e. the extent to which the device absorbs energy is a material and wavelength dependent parameter called the absorption coefficient. It thus helps in describing the energy propagation through a homogeneous system [25]. The absorption coefficient for silicon is poor since it is an indirect band gap material i.e. the bottom of the conduction band and the top of the valence band are not aligned at the same wave vector. This demands change in energy as well as momentum for the photon to be absorbed to generate carriers contributing to current thus reducing the probability for the absorption of photons and resulting in lower values of absorption coefficients.
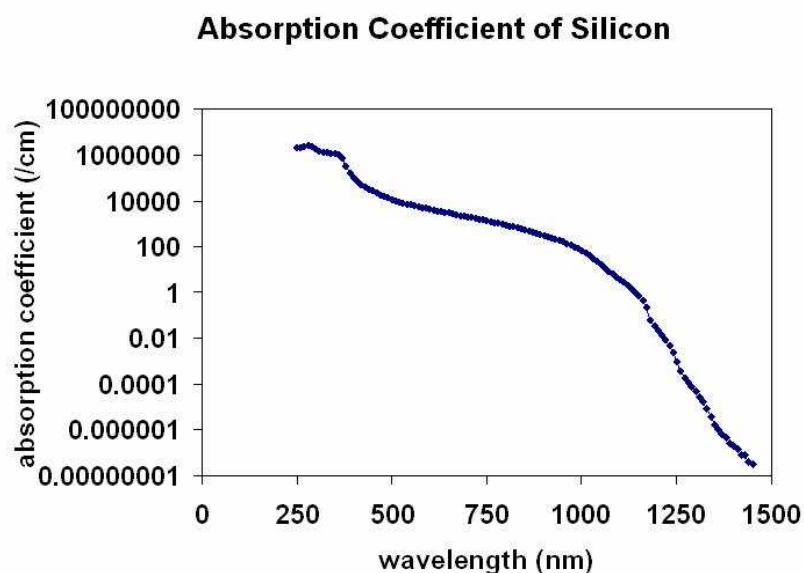

Figure 3.3 Absorption Coefficients Vs Wavelength for Silicon

The structure simulated to emulate the realistic solar cell is an n+-p-p+ structure with the p+ region forming the bottom contact and the n+ region forming the top surface. The structure is simulated for 25% and 50% of top metal and the rest of the window exposed to the solar radiation and prone to surface recombination phenomenon.
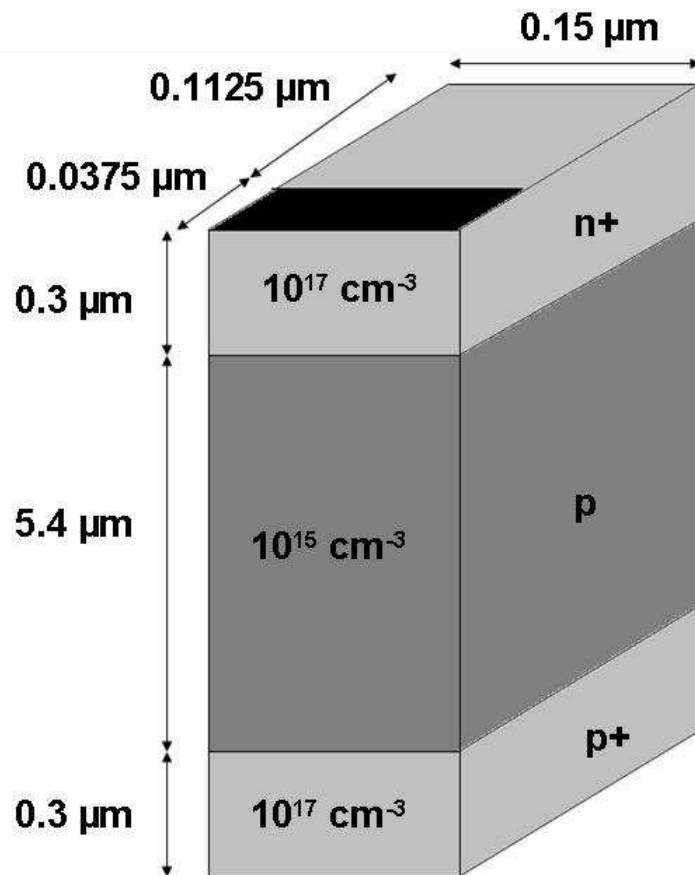

Figure 3.4 Simulated n+-p-p+ Silicon Solar cell structure

The structure is simulated for various base thicknesses i.e. 2.4µm, 5.4µm and 8.4µm. The solar radiation is incident normally onto the top surface and the metal is considered to be purely reflective in the simulation.

II.   SIMULATION RESULTS UNDER ILLUMINATION

Initial simulations were done on a pn-junction silicon solar cell as a one dimensional simulation to evaluate the use of drift diffusion modeling for solar cells. For a solar cell the I-V plot is in the fourth quadrant as was explained in Chapter 2. The current density vs. voltage plot obtained for the pn junction silicon solar cell is,
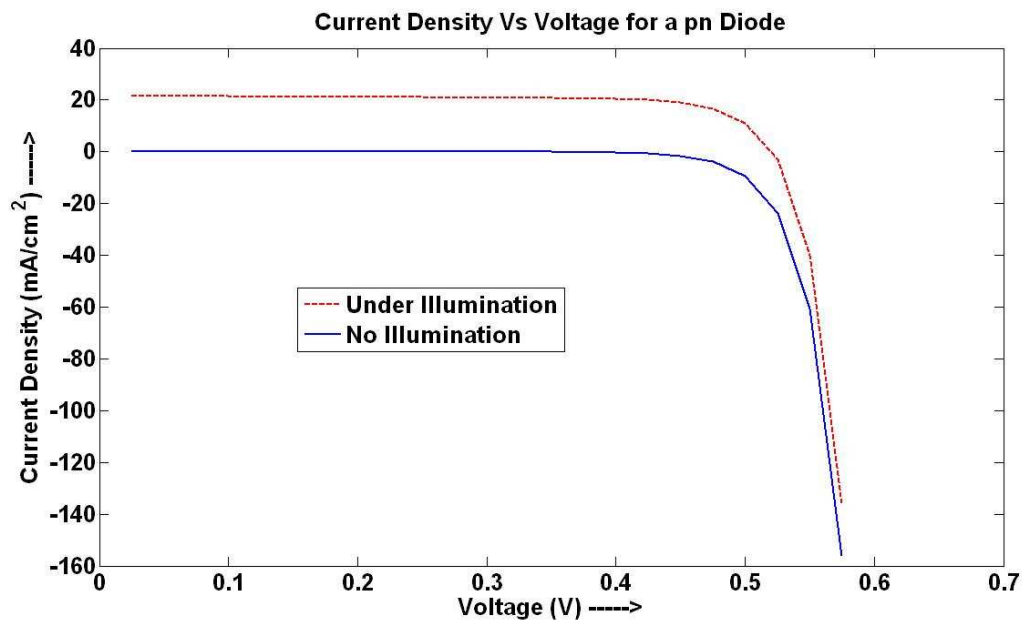

Figure 3.5 Current Density Vs Voltage for a pn junction Silicon Solar cell

In Figure 3.5 we observe that the plot has been flipped with respect to the X axis to represent the current density as positive values. Thus we see the shift the I-V plot when the device is illuminated and contributing to dark current. The open circuit voltage is around 0.55V and short circuit current density of around $20 \, mA/cm^2$.

From the simulations it is thus proved that drift diffusion modeling works fine in

solving for the current in a solar cell. Now the simulation was done on a more practical device i.e. n+-n-p+ structure with p+ forming the back contact. Initially transparent contacts were assumed with no shadowing or surface recombination. The equilibrium simulation results for the n+-p-p+ structure are,
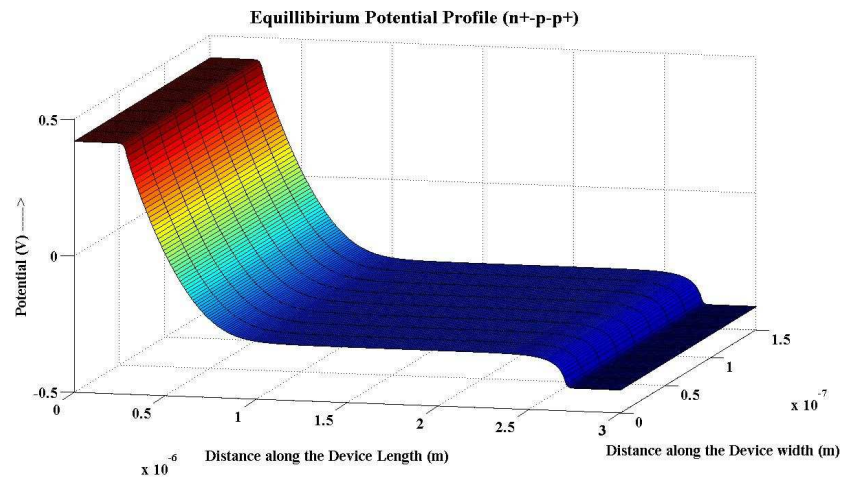

Figure 3.6 Equilibrium Potential Profile of an n+-p-p+ structure
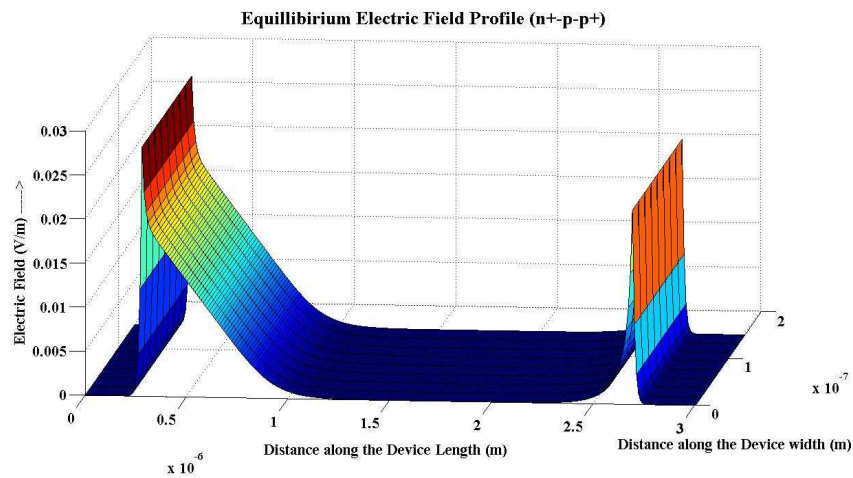

Figure 3.7 Equilibrium Electric Field of an n+-p-p+ structure

Figure 3.6 and 3.7 represent the Potential Profile and the Electric field respectively at Equilibrium i.e. with no applied bias. In this case only Poisson equation is solved to obtain the potential profile and the carrier densities related exponentially to the potential as no transport is involved. The equilibrium carrier densities are,
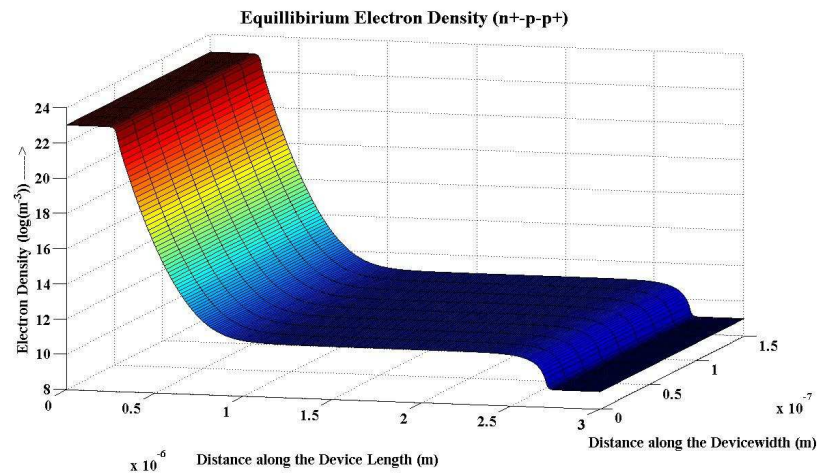

Figure 3.8 Equilibrium Electron Density Profile of an n+-p-p+ structure
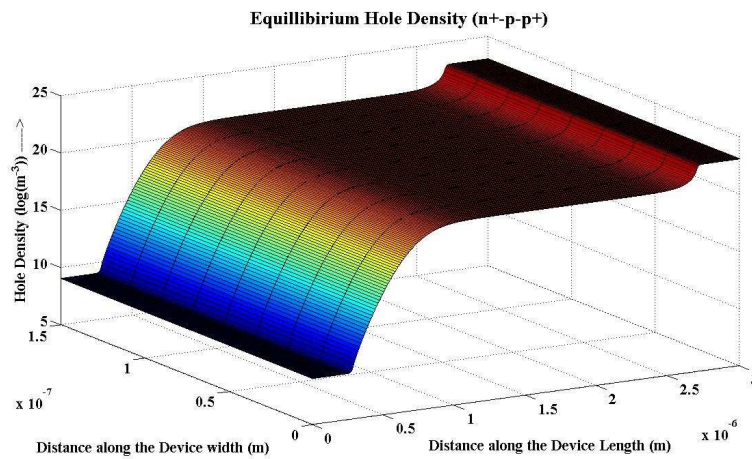

Figure 3.9 Equilibrium Hole Density Profile of an n+-p-p+ structure

Now the device is illuminated with one sun AM 1.5 and in this cases both Poisson and drift diffusion equations have to be solved self consistently since transport of carriers is involved leading to production of current. The generation recombination mechanisms included in this simulation are Auger recombination, thermal generation recombination, radiative recombination and generation due to the incoming light source. The carrier density profile under Illumination is,
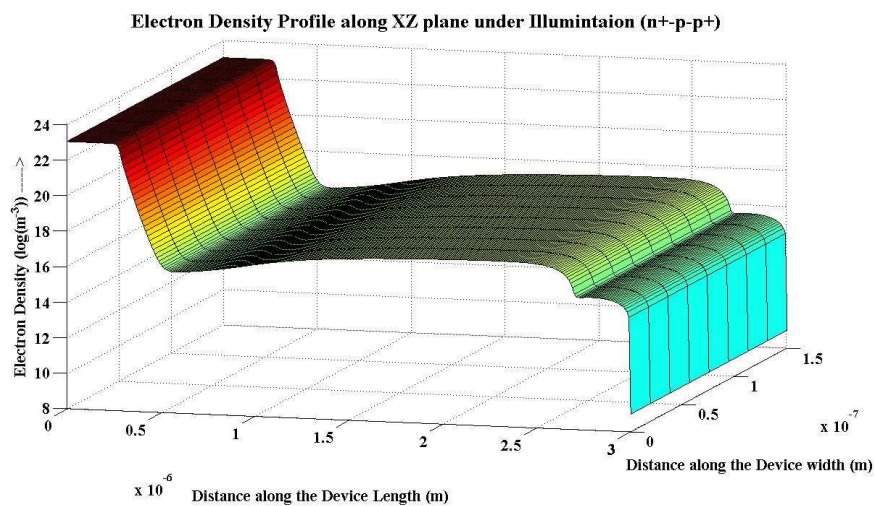

Figure 3.10 Electron Density Profile of an n+-p-p+ structure under Illumination

From Figure 3.10 we observe that there is an increase in the electron carrier density and this is seen in the p-base region and also the p+ region as the electron concentration in these regions are low. The generation of carriers is not high in the n+ region of the device due to high doping concentration of donors. The hole carrier density is also altered in a similar fashion by the incoming solar radiation as it produces equal number of electrons and holes. This can be observed in Figure 3.11,
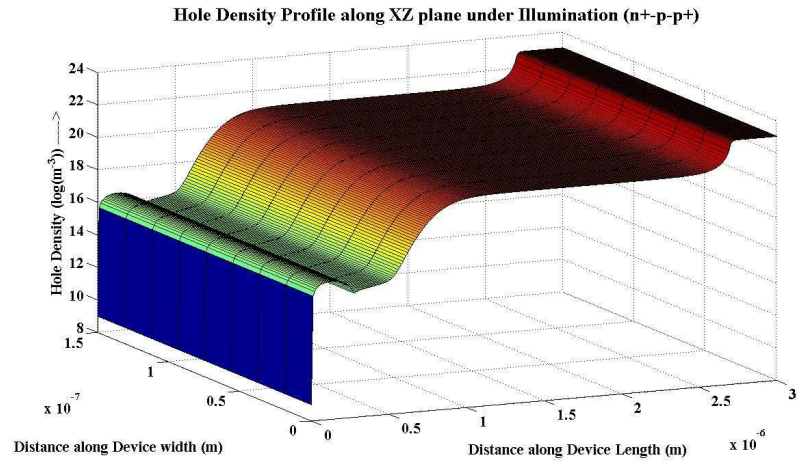
Figure 3.11 Hole Density Profile of an n+-p-p+ structure under Illumination

The potential profile under illumination as shown in Figure 3.12 is not very much visibly different from the equilibrium potential profile as simulated in Figure 3.6 i.e. it does not show a big difference as seen in the case of the carrier concentrations since the dependence of carrier densities on potential is exponential.
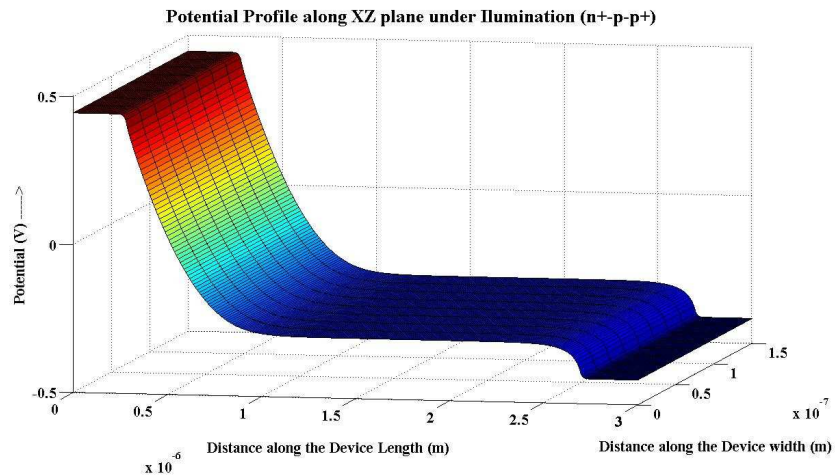

Figure 3.12 Potential Profile of an n+-p-p+ structure under Illumination

When solar radiation starts generating carriers in the device it tends to decrease the electric field in the depletion region and this is observed in the simulation. In Figure 3.13 the difference between the electric field before and after the simulation is taken.
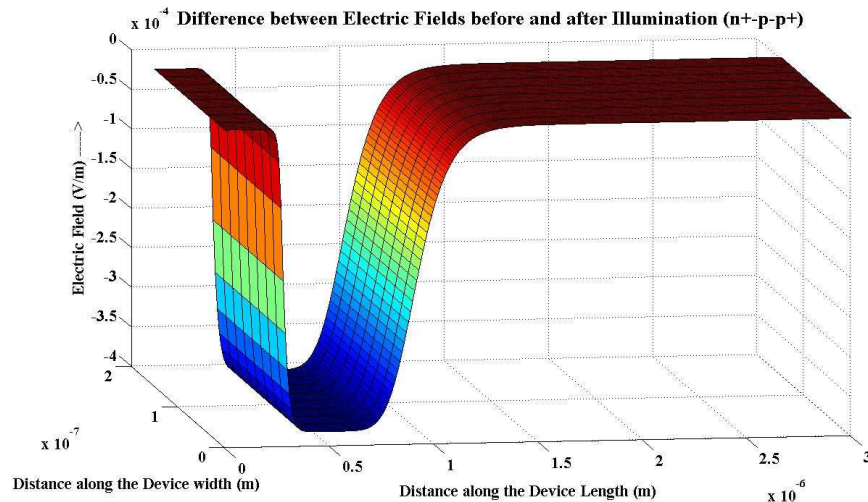

Figure 3.13 Difference in Electric field profile before and after simulation

We observe from Figure 3.13 that there is a reduction in the electric field and this complies with the concept of working of a solar cell. As solar radiation creates large number of carriers, these carriers tend to recombine with the charges in the depletion region and thus reduce the field.

Simulations were also done for a p+-p-n+ structure and similar results were extracted. Simulations were also done for varying widths of the base region for both n+-p-p+ structures and p+-p-n+ structures.
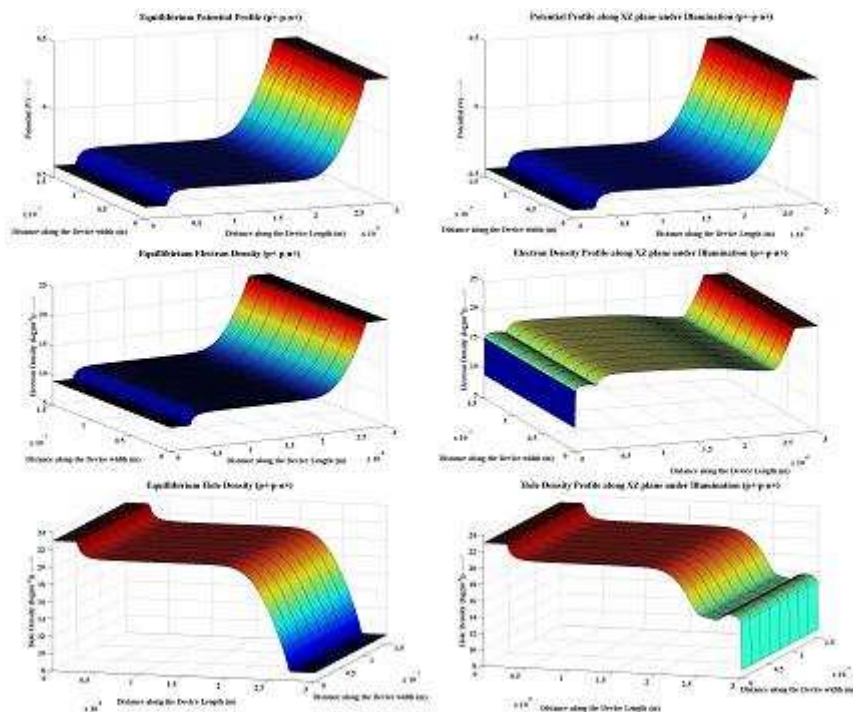
Figure 3.14 Simulations of Potential, Electron and Hole Density Carrier Profiles under no light and under Illumination

III.   SIMULATION RESULTS UNDER ILLUMINATION WITH SHADOWING AND SURFACE RECOMBINATION

The simulations presented in the previous section were under the assumption of transparent contacts but in reality the contacts are not 100% transparent and do posses some reflectivity. This tends to reduce the amount of solar radiation entering the device structure leading to reduced number of carrier generation resulting in decrease in efficiency of the solar cell. Thus, the top contacts are made to be optimally in small percentage in comparison to the window to allow maximum incoming radiation to go through the device. The window exposed has some defects in it and thus leads to surface

recombination effect. This also tends to reduce the efficiency of the solar cell as certain numbers of carriers are lost at the surface.

Simulation has been performed for contact areas of about 25 and 50% of the top surface. The carrier profile for a contact area of about 50% of the top surface for a base width of $5.4\,\mu m$ is,
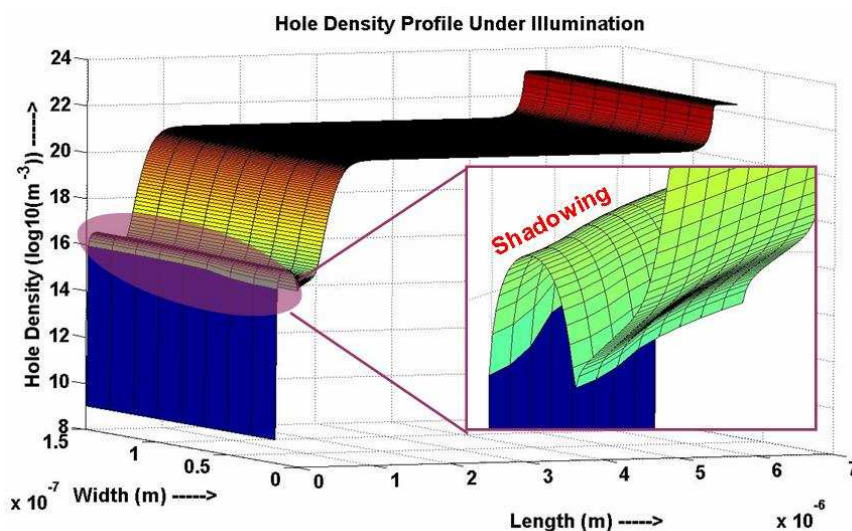

Figure 3.15 Hole Density Profile under Illumination with Shadowing (n+-p-p+)

We observe from Figure 3.15 that there is a gradient in the carrier density profile under the top metal contact. This is because there are a huge number of carriers that are generated due to the incoming solar radiation through the window and almost no generation under the metal contact (as in this simulation the metal is assumed to have 100% reflectivity) and therefore the carriers see a concentration gradient and tend to diffuse under the contact . Thus, Shadowing of the metal contact and surface

recombination phenomenon play a very important role in determining the efficiency of the solar cell.

IV.   EFFICIENCY CALCULATION AND TRENDS IN EFFICIENCY

The efficiency of the cell is calculated using the expression,

$$\eta = \frac{V_{oc} I_{sc} FF}{P_{in}}$$

where η represents the efficiency of the solar cell, V_{oc} is the open circuit voltage, I_{sc} represents the short circuit current, FF represents the Fill factor and P_{in} represents the input power of the incoming solar radiation and

$$P_m = V_{oc} I_{sc} FF$$

where P_m represents the maximum power [26]. The input power is calculated in the following way,

$$P_{in} = (\int_{\lambda_1}^{\lambda_2} P(\lambda) d\lambda) wh$$

where λ_1 and λ_2 represent the range of wavelengths which comprises the incoming solar radiation, w represents the width of the structure and h represents the height of the structure. This width and height are the dimensions of the window of the structure.

The efficiencies are calculated for the structures for various lengths of the base width i.e. $2.4\,\mu m$, $5.4\,\mu m$ and $8.4\,\mu m$. With the increase in the base width the efficiency goes up but the trend tends to start drop down after reaching a peak. By reducing the base thickness of the substrate the photo generated current decreases since the longer wavelength photons corresponding to lower energy travel longer distances before getting absorbed into the material. But by reducing the thickness of the substrate the efficiency also increases since the ratio of diffusion length to the thickness of the substrate increases and this enhances the collection efficiency of minority carriers [27]. Figure 3.16 shows the trend of efficiency with the base width thickness of the device,
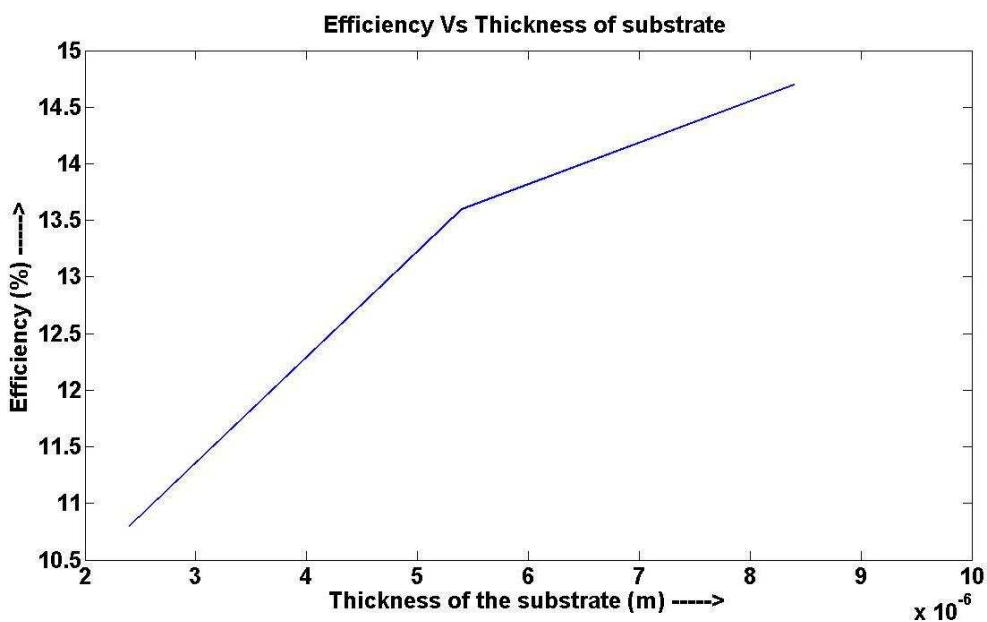

Figure 3.16 Efficiency Vs thickness of base (n+-p-p+)

The complete efficiency trend is not extracted and the simulation is done for a maximum thickness of $8.4\,\mu m$ due to extreme increase in simulation time with further increase in thickness of the base.

Chapter 4

CONCLUSIONS AND FUTURE WORK

I.   CONCLUSIONS

This chapter summarizes the key features of this research and its results. This is followed by the plan for future research work. Summarizing the work done, a Drift-Diffusion model has been utilized to model the working of a silicon solar cell. The self consistent solution of the potential and carrier distribution is obtained by the coupled solution of the Poisson equation and the continuity equations. The structures that were simulated were a p-n diode, p+-p-n+ structure and n+-p-p+ structure. These structures were simulated with transparent contacts and the generation of carriers was evident from the carrier density plots and also the I-V plot presented in the previous Chapter. The shadowing of the top contact plays a very important role as it decreases the total photogeneration rate in the device and thus changing the efficiency of the cell. The surface recombination phenomenon is also incorporated in the code in the exposed window region and this also causes the loss of carriers thus reducing the efficiency. The decrease in efficiency is observed from the transparent contact to the incorporation of shadowing and surface recombination effects. The efficiency of the device changes with the base region thickness since its ability to capture low energy photons (higher wavelengths) increases and thus increasing the efficiency but the efficiency starts decreasing after reaching a critical length. The increasing trend in efficiency was observed in simulation but the structure thickness was not increased enough to see the decreasing trend due to limitation of the simulation time.

II.   FUTURE WORK

The simulations presented here have been done on a silicon solar cell homojunction but the code is generalized to incorporate heterojunctions. Thus high efficiency solar cells can be effectively simulated using the above model. Photon Recycling has not been included in the present version of the code. Reverse leakage currents due to radiative recombination play a very significant role in the performance of a solar cell. The reduction of this current component plays a big role in increasing the open circuit voltage of the cell and thus the efficiency. Photon recycling helps in reducing the effective recombination rate when near band edge radiative recombination play a dominant role in the device [28].

The model used in the simulation of the device i.e. Drift Diffusion Model which has limitations that it is not a very good model for high field conditions and does not include scattering mechanisms as accurately as one can do in a particle based device simulators. The inclusion of thermal effects can also play a significant role in the working of a solar cell when operated under concentrated sunlight and this can also be done in a more proper way using particle based device simulation scheme as we have demonstrated recently on the description of the operation of FD SOI Devices. Thus, our ultimate goal is to move to a more detailed picture of transport in both single and multi-junction solar cells by utilizing particle based device simulations of solar cells in near future.

References

[1] G. W. Crabtree and N. S. Lewis, "Basic research needs for solar energy utilization," 2005.

[2] G. W. Crabtree and N. S. Lewis, "Solar Energy Conversion," *Physics Today,* vol. 60, pp. 37-42, 2007.

[3] J. Hakes, "Long term world oil supply (A resource Base/Production path analysis)," 2000.

[4] T. Key, "Solar photovoltaics: Expanding electric generation options," Electric Power Research Institute, 2007.

[5] Solar cell. http://en.wikipedia.org/wiki/Image:PVeff(rev110707)d.png#filehistory

[6] Solar cell - generations. http://en.wikipedia.org/wiki/Solar_cell#Second_Generation

[7] G. Gourdin, "Lecture notes: Solar cell technology (current state of the art)," 2007.

[8] M. A. Green, "Third generation photovoltaics: solar cells for 2020 and beyond," vol. 14, pp. 65-70, 2002.

[9] Third generation solar cell. http://en.wikipedia.org/wiki/Third_generation_solar_cell

[10] D. K. Schroder, "Lecture notes: Solar cells,"

[11] M. S. Lundstrom, "Numerical Analysis of Silicon Solar cells," 1980.

[12] J. L. Gray, "A computer model for the simulation of thin-film silicon-hydrogenalloy solar cells," *IEEE Transactions on Electron Devices,* vol. 36, pp. 906-912, 1989.

[13] E. K. Banghart, "Physical mechanisms contributing to nonlinear responsivity in silicon concentrator solar cells," 1989.

[14] P. D. DeMoulin and M. S. Lundstrom, "Projections of GaAs solar-cell performance limits based ontwo-dimensional numerical simulation," *IEEE Transactions on Electron Devices,* vol. 36, pp. 897-905, 1989.

[15] R. J. Schwartz, J. L. Gray and Y. J. Lee, "Design considerations for thin film CuInSe, and other polycrystalline heterojunction solar cells," in 1991, pp. 920-923.

[16] Silvaco. http://www.silvaco.com/

[17] Crosslight. http://www.crosslight.com/

[18] Synopsys. http://www.edn.com/article/CA6591928.html

[19] D. Vasileska and S. M. Goodnick, *Computational Electronics.* Morgan & Claypool Publishers, 2006,

[20] D. Vasileska. Lecture notes: Semiconductor device and process simulation. Available: http://www.eas.asu.edu/~vasilesk/

[21] J. R. Shewchuk. (1994, An introduction to the conjugate gradient method without the agonizing pain. Carnegie Mellon University,

[22] Conjugate gradient method. http://mathworld.wolfram.com/

[23] S. Selberherr, *Analysis and Simulation of Semiconductor Devices.* ,1st ed.Springer, 1984, pp. 308.

[24] D. Vasileska. Lecture notes : Semiconductor device and process simulation and quantum mechanics. Available: www.eas.asu.edu/~vasilesk

[25] Absorption coeffecient. http://en.wikipedia.org/wiki/Absorption_coeffecient

[26] M. A. Green, *Solar Cells.* Prentice Hall, 1982,

[27] W. P. Mulligan, M. D. Carandang, De Ceuster, Denis M., C. N. Stone and R. M. Swanson, "Reducing silicon consumption by leveraging cell efficiency," SunPower Corporation,

[28] S. M. Durbin and J. L. Gray, "Numerical Modeling of Photon Recycling in Solar Cells," *IEEE Transactions on Electron Devices,* vol. 41, 1994.